Genome-scale analysis of cellular restriction factors that inhibit transgene expression from adeno-associated virus vectors

Ashley M Ngo[1], Andreas S Puschnik[1,2]

[1] Chan Zuckerberg Biohub, San Francisco, CA, USA

[2] Correspondence should be addressed to A.S.P. (andreas.puschnik@czbiohub.org)

ABSTRACT

Adeno-associated virus (AAV) vectors are one of the leading platforms for gene delivery for the treatment of human genetic diseases, but the antiviral cellular mechanisms that interfere with optimal transgene expression are incompletely understood. Here, we performed two genome-scale CRISPR screens to identify cellular factors that restrict transgene expression from AAV vectors. Our screens revealed several components linked to DNA damage response, chromatin remodeling and transcriptional regulation. Inactivation of the Fanconi Anemia gene FANCA, the Human Silencing Hub (HUSH) associated methyltransferase SETDB1 and the gyrase, Hsp90, histidine kinase and MutL (GHKL)-type ATPase MORC3 led to increased transgene expression. Moreover, SETDB1 and MORC3 knockout improved transgene levels of several AAV serotypes as well as other viral vectors, such as Lentivirus and Adenovirus. Finally, we demonstrated that siRNA knockdown of SETDB1 and MORC3 prior to viral vector administration enhanced transgene expression, providing a strategy for the improvement of gene therapy applications.

23 **INTRODUCTION**

24 Adeno-associated virus (AAV) provides a powerful and versatile platform for gene delivery
25 to treat a variety of human genetic diseases. AAV is a small single-stranded DNA virus with a
26 genome size of ~4.7 kb from the *Parvoviridae* family. Its genome consists of two open reading
27 frames, *rep* and *cap*, which are flanked by inverted terminal repeat (ITR) sequences[1,2]. The ITRs
28 are the only cis-acting elements required for genome packaging, which enables the generation
29 of recombinant AAV (rAAV) vectors containing a reporter or therapeutic transgene in place of the
30 endogenous *rep* and *cap* genes[3]. rAAV vectors have been clinically approved for the treatment of
31 monogenic diseases, such as lipoprotein lipase deficiency, Leber congenital amaurosis and spinal
32 muscular atrophy, and there are over 150 ongoing clinical studies for additional rAAV-based
33 therapies[4].

34 Despite the recent clinical successes, rAAV-based gene therapies face several challenges:
35 (1) Large-scale manufacturing of rAAV for high dose administration (>10^{14} viral particles per
36 patient), is expensive and difficult; (2) immunological barriers such as the presence of pre-existing
37 neutralizing antibodies against AAV or the triggering of a robust humoral immune response upon
38 treatment prevent (repeated) administration; (3) hepatic and neuronal genotoxicity has been
39 observed in a number of high-dose administrations; (4) transgene expression can be lost over
40 time due to the clearance of transduced cells through a cytotoxic T cell response and/or potential
41 silencing of transgene expression[4–6].

42 Increased efficiency in rAAV transgene expression could therefore allow for a reduction
43 in the therapeutic doses needed, which consequently could decrease costs, elicit fewer
44 neutralizing antibodies, reduce the risk of genotoxicity, and lower AAV capsid-directed T

45 lymphocyte-mediated cytotoxicity. However, the precise host cellular pathways that restrict
46 rAAV transgene expression are incompletely understood.

47 To address this knowledge gap, we performed genome-wide CRISPR knockout (KO) and
48 interference (CRISPRi) screens to identify cellular factors that restrict transgene expression from
49 rAAV vectors. These identified several factors involved in DNA repair and chromatin regulation,
50 most prominently the Fanconi Anemia (FA) pathway, components of the Human Silencing Hub
51 (HUSH) complex and the gyrase, Hsp90, histidine kinase and MutL (GHKL)-type ATPase MORC3.
52 Follow-up studies demonstrated that genetic deletion of FANCA, the HUSH-associated
53 methyltransferase SETDB1 and MORC3 led to increased transgene expression from rAAV vectors.
54 SETDB1 and MORC3 were also shown to inhibit transgene expression from other virus-based
55 vectors such as Lentivirus and Adenovirus, suggesting that they represent a broad restriction
56 mechanism against foreign DNA elements. Finally, we demonstrated that treatment with siRNAs
57 against SETDB1 and MORC3 prior to rAAV or Lentivirus transduction led to increased transgene
58 expression in human cells, indicating that this strategy should be explored further for the
59 potential enhancement of viral vector-based gene therapy regimens.

60

61 **RESULTS**

62 **Genome-wide CRISPR screens identify rAAV restriction factors**

63 To identify cellular restriction factors of rAAV transgene expression that are likely to be
64 conserved across multiple cell types, we performed two parallel genome-wide screens using
65 CRISPR KO in A549 human alveolar basal epithelial cells and CRISPRi in K562 myeloid lymphoblast
66 cells. We used a non-saturating multiplicity of infection (moi) so that knockout/knockdown of a

67 repressor would lead to increased expression of a fluorescent reporter transgene. Based on rAAV
68 serotype 2 (AAV2) moi titrations, we used 10,000 viral genomes (vg)/cell for the A549 screen and
69 50,000 vg/cell for the K562 screen (Figure S1A). We performed two rounds of rAAV transduction
70 and FACS-based enrichment of the top 10-20% fluorescent CRISPR library cells followed by
71 analysis of the guide RNA (gRNA) representation via next-generation sequencing (Figure 1A).
72 Analysis with MaGeCK, a computational tool for CRISPR screen analysis, resulted in significant
73 enrichment of 20 genes in the A549 screen and of 88 genes in the K562 screens with a cutoff of -
74 log(enrichment score) >5 (Figure 1B and 1C, Supplemental Table 1). Nearly all individual gRNAs
75 were enriched for the top 15 genes of both screens, suggesting that the increased transgene
76 expression phenotypes resulting from the genetic perturbations were robust (Figure S1B). We
77 performed STRING analysis on the top 100 hits from both screens, which identified functional
78 gene clusters and cellular pathways, such as the FA pathway, the HUSH complex, the SMC5-SMC6
79 complex, the CCR4-NOT complex, and genes linked to DNA damage repair and chromatin
80 regulation (Figure 1D, Supplemental Table 2). Comparison of the enrichment scores from the
81 A549 and K562 CRISPR screens highlighted that a subset of the FA genes, the histone
82 methyltransferase SETDB1, the GHKL-type ATPase MORC3, SUMO Interacting Motifs Containing
83 1 (SIMC1), the DNA damage response gene ATM and other genes (SMCHD1, MTF1, DCLRE1A,
84 DAXX, FAM208A, ZRANB2) were significantly enriched in both datasets (Figure 1E and S1C).

85 The FA pathway is a biochemical network of 19 genes which are responsible for DNA
86 repair of interstrand crosslinks and stabilization of stalled replication forks, which can impede
87 DNA replication and transcription[7]. During this process, the FA core complex first recognizes the
88 DNA lesion before a nucleolytic incision occurs and the lesion is repaired through homologous

89 recombination. Most FA core complex components (FANCA-FANCM), which are responsible for
90 lesion recognition and binding, were robustly enriched in both rAAV screens, while the FA factors
91 mediating lesion resolution downstream and the homologous recombination machinery were
92 not or only partially enriched (Figure 1E). Another DNA damage repair factor, the
93 serine/threonine protein kinase ATM, activates checkpoint signaling upon double strand breaks,
94 apoptosis and genotoxic stresses, thereby acting as a DNA damage sensor[8]. Loss of the FA
95 pathway and ATM is synthetic lethal, suggesting closely linked cellular roles[9]. Several additional
96 DNA damage repair factors and components of the SMC5-SMC6 complex, which is involved in
97 genome stability and DNA repair, were strong hits only in the K562 screen (Figure 1E)[10].

98 Besides DNA damage response, many factors were linked to chromatin regulation (Figure
99 1E). The histone methyltransferase SETDB1 is recruited by the HUSH complex, composed of
100 FAM208A (also known as TASOR), MPHOSPH8 and PPHLN1, to heterochromatic loci and foreign
101 DNA elements, such as retroviruses and transposons, to mediate transcriptional repression[11,12].
102 Other associated factors (MORC2, ZNF638 and ATF7IP) required for recruitment and full
103 epigenetic silencing activity were also enriched in both screens[13–15]. Finally, MORC3 is a nuclear
104 matrix protein with ATPase activity and has been linked to gene silencing, including of viral
105 pathogens[16–18].

106 Overall, the screens identified numerous candidate restriction factors for rAAV transgene
107 repression, which have canonical roles in DNA damage repair and chromatin regulation. For
108 subsequent validation studies, we focused on the FA pathway due to the strongest phenotype
109 across both screens as well as SETDB1 and MORC3 due to their described function in silencing
110 certain viral pathogens.

111

112 **The Fanconi Anemia pathway suppresses transgene expression from rAAV vectors**

113 The FA pathway has to our knowledge not been functionally associated with the
114 regulation of AAV transgene expression. To validate the impact of the FA pathway on rAAV
115 transgene expression, we transduced three sets of FANCA expressing and matched FANCA
116 deficient cells, which were kindly provided by the Fanconi Anemia Research Fund at Oregon
117 Health & Science University. Dual gRNA/Cas9-mediated deletion of the N-terminus of FANCA in
118 UM-SCC-01 cells significantly increased the percentage of rAAV2-tdTomato positive cells
119 (rAAV2+) as well as their median fluorescence intensity (MFI) relative to WT cells (Figure 2A and
120 2B). This effect was reversed in FANCA transgene-complemented derivatives of the KO cells
121 (Figure 2A and 2B). Furthermore, transduction of mouse ear fibroblasts (MEFs) derived from WT
122 or FANCA KO 129S4/SvJaeSor mice showed a similar increase of rAAV transgene expression in the
123 FANCA-deficient background (Figure 2C and 2D). Lastly, we obtained FA patient derived head and
124 neck squamous cell carcinoma cells ("974 cells"), which harbor a FANCA frameshift mutation, as
125 well as corresponding FA patient cells that were lentivirally complemented with an intact FANCA
126 cDNA copy[19]. Complementation with FANCA cDNA led to a substantial decrease of rAAV
127 transgene expression relative to the FA patient derived 974 cells (Figure 2E and 2F). Together,
128 these data support that the FA pathway plays a role in the AAV life cycle and inhibits transgene
129 expression from rAAV vectors.

130

131 **Knockout of MORC3 and SETDB1 enhances rAAV transgene expression**

132 Next, we sought to validate the impact of the (GHKL)-type ATPase MORC3 and the histone
133 methyltransferase SETDB1 on rAAV as previous reports have shown antiviral functions for other
134 DNA viruses[11,15,17,18]. We generated two clonal A549 KO cells per gene. The MORC3 KO clones
135 harbored frameshift mutations in exon 1, while the SETDB1 KO clones contained a frameshift or
136 large deletion (-21bp) in exon 2 (Figure S2A). The generated KO cell lines did not show any growth
137 defects (Figure S2B). Infection of KO cells with rAAV2-tdTomato showed a substantial increase in
138 rAAV2+ cells (by 16-19% in MORC3 KO and by 22-23% in SETDB1 KO cells 3 days post-infection
139 (dpi)) as well as in MFI (by 2.7-3.3x in MORC3 KO and by 5.4-6.8x in SETDB1 KO cells 3dpi) relative
140 to WT cells (Figure 3A, 3B and S3). rAAV transgene expression remained higher in KO vs WT cells
141 over 8 days. Signal decreased in all conditions at later timepoints likely due to the dilution of
142 episomal rAAV DNA during cell proliferation. Lentiviral complementation of MORC3 KO cells with
143 MORC3 cDNA lowered the percentage of rAAV+ cells and MFI to levels observed in WT cells
144 (Figure 3C and 3D), supporting that rAAV transgene expression is directly modulated by MORC3
145 activity. Similarly, complementation of SETDB1 KO cells with SETDB1 cDNA decreased both the
146 percentage of tdTomato+ cells (albeit to a lesser degree) and MFI (Figure 3E and 3F). Finally, we
147 tested whether deletion of MORC3 or SETDB1 allowed for achieving comparable rAAV
148 transduction rates with reduced rAAV moi. Across a range of 100 to 100,000 vg/cell, MORC3 and
149 SETDB1 KO cells exhibited significantly higher transgene expression levels than WT cells,
150 demonstrating that only ~one-tenth of the rAAV amount was needed in KO cells to achieve
151 similar transgene expression levels as in WT cells (Figure 3G and 3H). This observation suggests
152 that a large fraction of rAAV genomes are readily silenced in WT cells and that inhibition of

153 MORC3 or SETDB1 activity could potentially decrease the amount of rAAV that is required for
154 therapeutic outcomes in gene replacement therapies.

155 As different rAAV serotypes are used in research and clinical applications, often
156 depending on the target cell type or tissue, we assessed whether MORC3 and SETDB1 also
157 affected transgene expression from different rAAV serotypes. We infected cells with rAAV1,
158 rAAV5 and rAAV6 vectors, which only lowly expressed GFP transgene in WT A549 cells. By
159 contrast, GFP expression was drastically increased in MORC3 and SETDB1 KO cells (Figure 4A and
160 4B). Moreover, rAAV vector genomes can be single-stranded (ssAAV), which require second-
161 strand synthesis prior to gene expression (as were all rAAV vectors used above), or they can be
162 constructed to be self-complementary (scAAV). These scAAV vectors form intra-molecular dsDNA
163 and thus do not require cell-mediated synthesis of the second strand. We observed that presence
164 of MORC3 and SETDB1 also restricted transgene expression from scAAV genomes, similarly as for
165 ssAAV vectors, which suggests that these cellular factors affect steps in the viral life cycle
166 downstream of second-strand synthesis (Figure 4C and 4D). Indeed, rAAV transgene mRNA levels
167 were moderately increased by 10-30% in MORC3 KO cells and by >100% in SETDB1 KO cells
168 (Figure S4A). In sum, we showed that MORC3 and SETDB1 negatively affect transgene expression
169 from different rAAV vectors by transcriptional silencing.

170

171 **Transgene expression from lentiviral and adenoviral vectors is also inhibited by MORC3 and**
172 **SETDB1**

173 In addition to rAAV, other viruses such as lentivirus and adenovirus are used for clinical
174 gene delivery applications[20]. Interestingly, several recent studies suggested that MORC3 and

175 SETDB1 can suppress expression of retroviral elements[11,18,21]. Consistent with previous studies,
176 both MORC3 and SETDB1 KO increased lentivirus transduction rates and MFI of GFP transgene
177 expression across multiple lentiviral dilutions (Figure 5A and 5B). This effect was overall
178 comparable as for rAAV, however, in contrast to rAAV, deletion of MORC3 had a stronger effect
179 on lentiviral transgene expression (~12x increase in MFI at 1:3 lentivirus dilution) than deletion
180 of SETDB1 (~8x increase in MFI). Real-time quantitative PCR (RT-qPCR) of lentiviral mRNAs
181 showed that de-repression of transgene expression levels was higher than for rAAV2 (Figure S4B).
182 During infection with GFP-expressing adenovirus 5 (AdV5-GFP), the percentage of GFP+
183 cells and the MFI of GFP were also increased in MORC3 and SETDB1 KO relative to WT cells (Figure
184 5C and 5D). By contrast, expression of a fluorescent protein from mRNA-liposomes was
185 unchanged in KO relative to WT cells (Figure 5E and 5F). Together, these data suggest MORC3
186 and SETDB1 broadly silence foreign DNA elements, such as viral vectors, regardless of whether
187 viral genomes are episomal or integrated in host genomic DNA.
188
189 **MORC3 and SETDB1 knockdown prior to viral vector delivery leads to increased transgene**
190 **expression**
191 To explore whether manipulation of MORC3 and/or SETDB1 activity could be harnessed
192 in a translational setting to improve transgene expression from viral vectors, we performed siRNA
193 knockdown prior to transduction of target cells. siRNAs have been clinically approved, e.g. for
194 several liver diseases, and could thus be used in conjunction with viral vectors to improve certain
195 gene therapy outcomes[22]. Transfection with MORC3 or SETDB1 siRNAs prior to rAAV2-tdTomato
196 transduction increased the percentage and MFI of tdTomato+ cells (Figure 6A and 6B).

197 Importantly, the combination of both siRNAs led to a synergistic effect increasing the MFI by ~3x
198 relative to a non-targeting siRNA (compared to 1.4x for MORC3 siRNA and 1.5x for SETDB1 siRNA
199 alone). Similarly, the use of siRNAs against MORC3 and SETDB1 increased the percentage and
200 MFI of transgene expression from a lentiviral vector (increase of MFI: 1.9x for MORC3, 1.7x for
201 SETDB1 and 4.8x for MORC3+SETDB1) (Figure 6C and 6D). In summary, knockdown (or possibly
202 pharmacological inhibition) of cellular restriction factors prior to viral vector administration can
203 enhance transgene expression in human cells.
204
205 **DISCUSSION**
206 Our genome-wide CRISPR screens provide a comprehensive picture of the cellular factors
207 that counteract gene expression from AAV vectors in human cells. The majority of the identified
208 host genes have known functions in DNA damage sensing and repair, chromatin remodeling and
209 transcriptional regulation. The most prominent hit across both CRISPR screens was the FA
210 pathway, which is critical for the resolution of interstrand crosslinks or stalled replication forks[7].
211 It is plausible that the ITRs in the AAV genome mimic interstrand crosslinks or stalled replication
212 forks and are thus recognized by the FA machinery, which subsequently may impede second-
213 strand synthesis of or transcription from the AAV genome. Interestingly, another study found
214 that deletion of FANCM led to enhanced AAV template-mediated homologous recombination[23].
215 This further supports that the FA machinery engages with AAV genomes to interfere with both
216 transgene expression as well as AAV template-mediated DNA repair. Other DNA damage
217 response genes enriched in our dataset, e.g. the ATM kinase and the MRN complex (consisting
218 of MRE11A/RAD50/NBN), have been shown to interact with the ITRs in the AAV genome and

219 suppress transgene expression[24–26]. Future studies are warranted to mechanistically investigate
220 how the FA pathway interferes with the AAV life cycle and whether FA components directly bind
221 to the AAV genome.

222 Moreover, we found that knockout of the histone methyltransferase SETDB1 substantially
223 increased transgene expression from rAAV and other viral vectors, such as lentivirus and
224 adenovirus. SETDB1 is recruited by the HUSH complex to regulate heterochromatin in
225 mammalian cells and has been described to mediate silencing of human immunodeficiency virus
226 (HIV) and other retroviral sequences by depositing repressive H3K9me3 histone marks[11,12,15,27,28].
227 Importantly, SETDB1 is able to silence both integrated and unintegrated retroviral DNA[11,15]. rAAV
228 genomes typically exist as unintegrated episomes and are thought to be bound by histones,
229 which can undergo hypermethylation leading to reduced gene expression[29]. SETDB1 and the
230 HUSH complex may thus be major contributors to rAAV chromatinization and silencing. Other
231 factors associated with HUSH recruitment and regulation of its activity were also enriched in our
232 screens. For example, ATF7IP interacts with SETDB1 and protects it from proteasomal
233 degradation in the nucleus, thereby maintaining SETDB1-mediated H3K9 trimethylation
234 activity[14]. The DNA-binding protein ZNF638 (also known as NP220) was shown to be responsible
235 for recruitment of the HUSH complex to unintegrated retroviral DNA and may also facilitate
236 recruitment to AAV genomes[15]. MORC2 was shown to be recruited by the HUSH complex to
237 heterochromatic sites, where its ATPase activity is required to mediate transgene silencing and
238 maintain chromatin compactness[13]. The role of the HUSH complex as a rAAV restriction factor
239 was also corroborated by a recent study. Consistent with our data, it showed that knockout of
240 HUSH components resulted in increased rAAV transgene levels and that deletion of ZNF638

241 (NP220) decreased repressive H3K9me3 histone marks on AAV genomes[30]. Together, the findings
242 provide compelling evidence that the HUSH machinery silences rAAV genomes in a similar
243 manner as previously demonstrated for retroviral DNA elements.

244 In addition to the HUSH-associated MORC2, MORC3, another Microchidia CW-type zinc
245 finger protein, was the top hit in the A549 screen and strongly enriched in the K562 screen. MORC
246 proteins are highly conserved, reside in the nucleus, contain a GHKL ATPase domain, and have
247 been linked to heterochromatin condensation and gene silencing[16,31]. Previously, MORC3 was
248 shown to restrict herpesviruses and endogenous retroviruses (ERVs)[17,18]. Mechanistic studies
249 revealed that MORC3 bound to ERV sequences and that knockout of MORC3 resulted in ERV de-
250 repression, reduced H3K9me3 levels and increased chromatin accessibility[18]. According to our
251 results, we propose that MORC3 is a critical rAAV restriction factor that silences rAAV genomes
252 through possible chromatin regulation.

253 Additional screen hits have also been linked to chromatin regulation and gene silencing.
254 The ATRX/DAXX complex is responsible for deposition of H3.3 histones at heterochromatic
255 regions and has been shown to associate with both SETDB1 and MORC3[18,32,33]. Moreover, the
256 CHAF1 complex, together with the histone chaperon ASF1, delivers newly synthesized H3/H4
257 dimers to replication forks and was recently shown to mediate silencing of unintegrated HIV-1
258 DNA[34,35]. Overall, these chromatin modifiers with described roles in foreign DNA silencing and
259 may therefore also be involved in rAAV repression.

260 Lastly, the SMC5-SMC6 complex, which is critical for genome stability and DNA repair[36],
261 has emerged as a component of antiviral responses. It has recently been linked to transcriptional
262 restriction of numerous DNA viruses, such as hepatitis B virus, unintegrated retroviral DNA,

263 papillomavirus and Epstein-Barr virus[37–40]. Our data suggests that SMC5-SMC6 can also potently
264 inhibit rAAV vectors. During DNA repair, this complex is recruited to DNA lesions by FAM178A
265 (also known as SLF2) and SLF1[41]. A recent preprint demonstrated that SIMC1, a top hit in both
266 CRISPR screens and largely with unknown function, forms a distinct complex with FAM178A to
267 localize SMC5/SMC6 to viral replication centers[42]. Therefore, it is plausible that rAAV is repressed
268 by recruitment of the SMC5-SMC6 complex via FAM178A/SIMC1.

269 Overall, the identification of multiple components of specific cellular pathways in our
270 CRISPR screens indicates that these are high-confidence candidates for rAAV restriction factors.
271 Of note, two previous siRNA screens for regulators of rAAV transduction in HeLa cells showed
272 enrichment of a subset of the same restriction factors as in our CRISPR screens, including ATF7IP,
273 CHAF1A, DAXX, NPAT (a positive regulator of ATM) and MORC3 (previously named ZCWCC3) in
274 one study, as well as ATF71P, CHAF1A, SETDB1, NPAT and the transcription factor MTF1 in
275 another study[43,44]. Thus, our work corroborates some previously identified candidate restriction
276 factors and expands the network of cellular factors that interfere with rAAV transgene
277 expression.

278 Finally, several studies have demonstrated viral countermeasures to some of the cellular
279 restriction mechanism described above. For example, both the HIV-1 protein Vpr and the
280 hepatitis B virus X protein antagonize SMC5-SMC6 activity[39,40]; HIV-2 Vpx counteracts HUSH
281 components[45]; and the HSV-1 protein ICP0 degrades MORC3[17]. As rAAV vectors lack any viral
282 proteins, they are likely to be more vulnerable to antiviral silencing mechanisms. A deeper
283 understanding of the key players and processes can thus provide new strategies to avoid cellular
284 sensing of AAV genomes and repression of viral transcription. Together with other approaches,

285 such as capsid engineering and the design of synthetic enhancers/promoters[46], the modulation
286 and evasion of host cell restriction factors has the potential to enhance viral vector gene therapy
287 applications.
288

289 **ACKNOWLEDGMENTS**
290 We thank Drs. Nicole Paulk (UCSF), Jan Carette (Stanford University) and James Zengel (Stanford
291 University) for helpful discussions; the Biohub Genomics Platform for help with sequencing of the
292 CRISPR screen samples; the UNC Gene Therapy Center for providing rAAV vectors; Drs. Jonathan
293 Weissman (UCSF) and Feng Zhang (Broad Institute) for providing the CRISPRi and CRISPR KO
294 library plasmids; and Dr. Leslie Wakefield and the Fanconi Anemia Research Fund at Oregon
295 Health & Science University for providing FANCA KO and trans-complemented cell lines.
296

297 **DATA AVAILABILITY**
298 The raw sequencing data for the A549 CRISPR KO and K562 CRISPRi screens are available on NCBI
299 under the BioProject ID PRJNA852611.
300

301 **MATERIAL AND METHODS**

302 **Cell Culture**
303 A549 and K562 were obtained from ATCC and cultured in DMEM (Gibco) supplemented with 10%
304 fetal bovine serum (Omega Scientific), penicillin/streptomycin (Gibco), non-essential amino acids
305 (Gibco) and L-glutamine (Gibco) at 37C and 5% CO2. HEK293ft cells were obtained from Thermo
306 Scientific and cultured as described above. WT, FANCA KO and trans-complemented FANCA KO

307 UM-SCC1 cells, WT and FANCA KO mouse ear fibroblasts, and FANCA-deficient patient-derived
308 974 cells with and without FANCA complementation were kindly provided by the Fanconi Anemia
309 Research Fund at Oregon Health & Science University and cultured as described above.
310
311 **Viruses**
312 The following rAAV vectors were obtained from the UNC School of Medicine Gene Therapy
313 Center Vector Core: AAV serotype 2 expressing GFP under a chimeric CMV–chicken ß–actin (CBA)
314 promoter (rAAV2-GFP), AAV serotype 2 expressing tdTomato under a CMV immediate
315 enhancer/β-actin (CAG) promoter (rAAV2-tdTomato), AAV serotype 1, 5 or 6 expressing GFP
316 under a CMV promoter (rAAV1/5/6-GFP), and self-complementary AAV serotype 2 expressing
317 GFP under a CMV promoter (scAAV2-GFP).
318 Lentivirus expressing GFP was produced by co-transfection of HEK293ft cells with the following
319 plasmids: plenti-CMV-Puro-DEST (Addgene #17452, gift from Eric Campeau & Paul Kaufman)
320 where GFP cDNA was cloned into the EcoRV site using NEBuilder HiFi DNA Assembly Master Mix;
321 pCMV-dR8.2 dvpr (Addgene, #8455, gift from Bob Weinberg); pCMV-VSV-G (Addgene, #8454, gift
322 from Bob Weinberg); and pAdVAntage (Promega). Supernatants were collected 48h post-
323 transfection, filtered and stored at -80C until use.
324 Adenovirus Serotype 5, Clone Ad5-CMV-hACE2/RSV-eGFP (NR-52390) was kindly provided
325 through BEI Resources.
326
327 **CRISPR screens**

328 A549 cells were stably transduced with lentivirus from lentiCas9-Blast (Addgene #52962, gift
329 from Feng Zhang) and subsequently selected using blasticidin. Next, a total of 240 million A549-
330 Cas9 cells were transduced with the lentivirus of the human GeCKO v2 library (Addgene
331 #1000000049, gift from Feng Zhang)[47] at a moi of 0.4 and selected using puromycin for 7 days.
332 60 million cells of the A549 CRISPR KO library were collected for genomic DNA (gDNA) extraction
333 to assess the reference gRNA distribution. Another 60 million cells were transduced with rAAV2-
334 GFP at a moi of 10,000 vg/cell, which resulted in a ~45-50% transduction rate. The top 10-15%
335 GFP+ cells were sorted 3 dpi and replated. After 7 days, the A549 cells were re-transduced with
336 10,000 vg/cell and the top 10-15% GFP+ cells were sorted again. A total of ~8 million cells was
337 collected for gDNA extraction.
338 K562-dCas9-KRAB cells were a gift from Jonathan Weissman. 240 million cells were transduced
339 with lentivirus from the Human Genome-wide CRISPRi-v2 (Addgene #83969, also gift from
340 Jonathan Weissman)[48] at a moi of 0.4 using spin-inoculation (1000g, 33C, 2h) in 6-well plates.
341 Subsequently, cells were selected using Puromycin for 5 days. 100 million K562 CRISPRi library
342 cells were collected for gDNA extraction to assess the initial gRNA distribution. Another 60 million
343 cells were spin-infected (1000g, 33C, 2h) with AAV2-GFP at a moi of 50,000 vg/cell. The top 15-
344 20% GFP+ cells (out of a total %GFP+ of 60%) were sorted and then continued to be cultured.
345 After 7 days, another round of spin-infection with AAV2-tdTomato and FACS of the top 10-15%
346 tdTomato+ cells were performed. A total of 16 million cells were collected for gDNA extraction.
347 For both A549 and K562 cells, gDNA was isolated using the Qiagen DNA Blood Maxi kit (for
348 reference cells) or multiple QIAamp DNA Mini kit columns (for sorted cells). CRISPR gRNA
349 encoding DNA sequences were amplified in a two-step nested PCR using KAPA HiFi HotStart

350 ReadyMixPCR Kit (Kapa Biosystems). In the first PCR step, 36-48 reactions and 12 reactions
351 containing 6 µg gDNA were set up for the reference and sorted samples, respectively, and
352 amplified for 16 cycles. Reactions for each sample were pooled and mixed. In the second PCR
353 step, 4 reactions containing 5 µl PCR1 product were amplified for 12 cycles using indexed primers.
354 PCR products were gel purified using QIAquick Gel Extraction Kit and sequenced on an Illumina
355 NextSeq 500 using custom sequencing primers. Primers sequences are listed in Supplemental
356 Table 3.
357 For analysis, demultiplexed FASTQ files were aligned to gRNA reference table and enrichment of
358 each gRNA was calculated by comparing the relative abundance in the selected and unselected
359 cell population. Gene enrichment analysis was performed using MaGeCK[49]. For STRING analysis[50],
360 the top 100 enriched genes from each CRISPR screen were used as input and gene interactions
361 were computed using a STRING confidence score of 0.4. MaGeCK scores were overlaid using
362 Cytoscape 3.9.0[51] and only the major gene network is displayed in Figure 1.
363
364 **Generation of KO cell lines**
365 DNA oligos (Integrated DNA Technologies) containing gRNA sequences complementary to
366 MORC3 or SETDB1 genomic loci were annealed and ligated into pX458 (Addgene #48138, gift
367 from Feng Zhang). A549 cells were transfected with pX458 constructs using Lipofectamine 3000
368 and two days later GFP-positive cells were single-cell sorted into 96-well plates containing
369 complete media. After several weeks, gDNA was isolated from obtained cell clones using
370 QuickExtract (Lucigen), the gRNA-targeted sites were PCR-amplified, PCR products Sanger-

371 sequenced and sequences aligned to reference sequences using Geneious Prime. A list of all used
372 gRNA oligo and genotyping primer sequences can be found in Supplemental Table 3.
373
374 **Lentiviral complementation of KO cells**
375 For generation of trans-complemented cell lines, lentivirus was generated as described above
376 using plenti-CMV-Puro-DEST containing MORC3 (OriGene Technologies, RC210530) or SETDB1
377 (OriGene Technologies, RC226620) cDNA sequences. KO cells were transduced in presence of
378 polybrene and subsequently selected using Puromycin.
379
380 **Flow cytometry**
381 Cells were plated in 96-wells and infected the next day. At indicated timepoints, cells were
382 trypsinized and analyzed by flow cytometry using a Cytoflex S flow cytometer (Beckman Coulter).
383 At least 4,000 cells were recorded per sample and cells were gated based on FSC/SSC, FSC-H/FSC-
384 A (singlets) and finally PE (tdTomato) or FITC (GFP) to determine the percentage of fluorescent
385 (infected) cells using FlowJo 10. Moreover, the median fluorescence intensity (MFI) of the
386 fluorescent cells was determined using FlowJo 10. In all experiments, uninfected cells served as
387 negative control for gate setting.
388
389 **RT-qPCR**
390 AAV- or lentivirus infected cells were then harvested using the Power SYBR Green Cells-to-CT kit
391 (Invitrogen). After reverse transcription, quantitative PCR was performed on a Bio-Rad CFX96

392 Touch system and viral transgene levels (GFP or tdTomato) were normalized to cellular 18S levels.
393 QPCR primer sequences can be found in Supplemental Table 3.
394
395 **Cell proliferation assay**
396 WT, MORC3 KO and SETDB1 KO cells were seeded in 96-wells at a density of 8,000 cells per well.
397 At 24, 48 and 72h post-plating Cell Titer Glo 2.0 solution (Promega) was added on top of the cell
398 media and incubated for 10min. After that, 100 µl were transferred to a white 96-well microplate
399 and luminescence was measured using on an EnVision plate reader (PerkinElmer).
400
401 **siRNA transfection**
402 ON-TARGETplus Non-targeting Control Pool, ON-TARGETplus Human MORC3 siRNA SMART POOL
403 and ON-TARGETplus Human SETDB1 siRNA SMART POOL were obtained from Horizon Discovery.
404 Cells were plated in 96-wells at ~70% confluency. The next day, siRNAs were complexed with
405 Lipofectamine RNAiMAX Transfection Reagent (Invitrogen) by mixing 25 µl OptiMEM (Gibco) with
406 1.5 µl RNAiMAX reagent and 25 µl OptiMEM with 0.5 µl siRNA (10 µM) per 96-well before
407 combining. After a 5 min incubation, the transfection mix was added to the cells. 2 days later the
408 siRNA transfection was repeated. After 4h the media was removed and cells were infected with
409 AAV or lentivirus.
410
411

412 **FIGURE LEGENDS**

413 **Figure 1. CRISPR screens reveal cellular factors that restrict rAAV transgene expression.**

414 (A) Schematic of genome-wide CRISPR screens using CRISPR KO in A549 lung epithelial cells or
415 CRISPRi in K562 lymphoblast cells. Cells were transduced with rAAV2 expressing a fluorescent
416 reporter gene (GFP or tdTomato) and the top 10-20% fluorescent cells were sorted by FACS.
417 After 5-7 days, a second round of transduction and sorting was performed before cells were
418 collected for analysis of sgRNA enrichment by next-generation sequencing.

419 (B) MaGeCK gene enrichment analysis of A549 CRISPR KO screen. Genes with -log10 (enrichment
420 score) > 5 are highlighted in blue.

421 (C) MaGeCK gene enrichment analysis of K562 CRISPRi screen. Genes with -log10 (enrichment
422 score) > 5 are highlighted in blue.

423 (D) STRING network for the top 100 hits from both the A549 and the K562 CRISPR screens. Genes
424 were clustered based on high-confidence interactions (STRING confidence cutoff 0.7) and the
425 major gene network is displayed. CRISPR screen enrichment scores for each gene are shown
426 using a color scale. Line thickness indicates confidence of interaction.

427 (E) Heatmap of gene rankings in A549 and K562 CRISPR screens for selected genes related to
428 DNA damage response and other cellular processes.

429

430 **Figure 2. The Fanconi Anemia pathway represses rAAV transgene expression.**

431 (A) rAAV2-tdTomato infection rate or (B) MFI of human WT, FANCA KO and KO UM-SCC1 cells
432 complemented with FANCA transgene (Tg). Cells were infected with rAAV2 (moi=10,000) for 48h
433 and tdTomato expression was analyzed by flow cytometry.

434 (C) rAAV2-tdTomato infection rate or (D) MFI of mouse ear fibroblasts (MEF) derived from WT or
435 FANCA KO 129S4/SvJaeSor mice. Cells were infected with rAAV2 (moi=100,000) for 24h and
436 tdTomato expression was analyzed by flow cytometry.
437 (E) rAAV2-tdTomato infection rate or (F) MFI of FA patient-derived head and neck squamous cell
438 carcinoma cells (974 cells), which harbor a FANCA frameshift mutation, as well as of 974 cells that
439 were complemented with FANCA transgene (Tg). Cells were infected with rAAV2 (moi=10,000)
440 for 48h and tdTomato expression was analyzed by flow cytometry.
441 All data are shown as the mean ± s.d. from biological triplicates. P-values were determined by
442 an unpaired t-test and are defined as follows: ns: non-significant; *: <0.05; **: <0.01; ***:
443 <0.001; ****: <0.0001.
444
445 **Figure 3. Knockout of MORC3 and SETDB1 increases rAAV2 transgene expression.**
446 (A) Percentage or (B) MFI of rAAV2-positive cells over time. WT, MORC3 KO or SETDB1 KO A549
447 cells were infected with tdTomato-expressing rAAV2 (moi=10,000) and cells were measured by
448 flow cytometry at day 1, 3, 6 and 8 post-infection.
449 (C) Percentage or (D) MFI of rAAV2-positive WT, MORC3 KO or cDNA-complemented MORC3
450 KO cells. Cells were infected with tdTomato-expressing rAAV2 (moi=10,000) and cells were
451 measured by flow cytometry 24 hpi.
452 (E) Percentage or (F) MFI of rAAV2-positive WT, SETDB1 KO or cDNA-complemented SETDB1 KO
453 cells. Cells were infected with tdTomato-expressing rAAV2 (moi=10,000) and cells were
454 measured by flow cytometry 24 hpi.

455 (G) Percentage or (H) MFI of rAAV2-positive WT, MORC3 KO or SETDB1 KO cells infected with
456 different multiplicities of infection (moi) and measured by flow cytometry 24 hpi.
457 Data are shown as the mean ± s.d. from biological triplicates (A-F) or from biological duplicates
458 (G-H). P-values were determined by an unpaired t-test and are defined as follows: ns: non-
459 significant; *: <0.05; **: <0.01; ***: <0.001; ****: <0.0001.
460
461 **Figure 4. MORC3 and SETDB1 restrict transgene expression from different rAAV serotypes as**
462 **well as self-complementary rAAV vectors.**
463 (A) Percentage or (B) MFI of WT, MORC3 KO or SETDB1 KO A549 cells infected with rAAV
464 serotypes 1, 5 or 6 (moi=50,000) and analyzed by flow cytometry at 3 dpi.
465 (C) Percentage or (D) MFI of WT, MORC3 KO or SETDB1 KO A549 cells infected with scAAV
466 serotype 2 (moi=10,000) and analyzed by flow cytometry at 3 dpi.
467 All data are shown as the mean ± s.d. from biological triplicates. P-values were determined by
468 an unpaired t-test and are defined as follows: ns: non-significant; *: <0.05; **: <0.01; ***:
469 <0.001; ****: <0.0001.
470
471 **Figure 5. MORC3 and SETDB1 repress transgene expression from lentiviral and adenoviral**
472 **vectors.**
473 (A) Percentage or (B) MFI of WT, MORC3 KO or SETDB1 KO A549 cells transduced with different
474 dilutions of a GFP-expressing lentivirus. Fluorescent cells were measured by flow cytometry 3
475 days post-transduction.

476 (C) Percentage or (D) MFI of WT, MORC3 KO or SETDB1 KO A549 cells infected with different
477 moi of a GFP-expressing adenovirus 5 (AdV5-GFP) vector. Cells were analyzed by flow
478 cytometry at 24 hpi.
479 (E) Percentage or (F) MFI of WT, MORC3 KO or SETDB1 KO A549 cells transfected with in-vitro
480 transcribed RFP mRNA and analyzed by flow cytometry 24 hpi.
481 All data are shown as the mean ± s.d. from biological triplicates.
482
483 **Figure 6. siRNA knockdown of MORC3 and SETDB1 prior to viral vector treatment enhances**
484 **transgene expression.**
485 (A) Percentage or (B) MFI of rAAV2-tdTomato positive A549 cells that were transfected with a
486 non-target siRNA or siRNAs against MORC3 and SETDB1 48h and again 4h prior to infection.
487 Cells were measured by flow cytometry 48hpi.
488 (C) Percentage or (D) MFI of lentiviral GFP expression levels in A549 cells that were transfected
489 with a non-target siRNA or siRNAs against MORC3 and SETDB1 48h and again 4h prior to
490 infection. Cells were measured by flow cytometry 48hpi.
491 All data are shown as the mean ± s.d. from biological triplicates. P-values were determined by
492 an ordinary one-way ANOVA test and are defined as follows: ns: non-significant; *: <0.05; **:
493 <0.01; ***: <0.001; ****: <0.0001.
494
495 **SUPPLEMENTAL FIGURES AND TABLES:**
496 **Figure S1. rAAV CRISPR screen optimization and analysis.**

497 (A) Moi titration of rAAV2-GFP on A549 and K562 cells. Infection rate was measured by flow
498 cytometry 24hpi.
499 (B) Log-fold changes (LFC) of individual gRNAs of the top 15 scoring genes from the A549 and
500 K562 CRISPR screens.
501 (C) Comparison of CRISPR screen enrichment scores from A549 and K562 screen.
502
503 **Figure S2. Characterization of MORC3 and SETDB1 KO cell lines.**
504 (A) Genotyping data of clonal MORC3 and SETDB1 KO cell lines. gRNA-targeted genomic loci
505 were amplified by PCR, products were Sanger-sequenced, and reads were aligned to
506 reference sequences.
507 (B) Cell proliferation of WT and clonal KO cell lines. Cells were harvested at each timepoint and
508 cell proliferation was measured by Cell Titer Glo assay. Data is displayed as mean ± s.d. from
509 biological triplicates.
510
511 **Figure S3. Representative flow cytometry data for rAAV2-tdTomato infection of WT, MORC3**
512 **KO and SETDB1 KO A549 cells.** Cells were infected with tdTomato-expressing rAAV2
513 (moi=10,000) and measured by flow cytometry at 3dpi. Each panel represents one biological
514 replicate. Summary data are displayed in Figure 3A and 3B.
515
516 **Figure S4. Knockout of MORC3 and SETDB1 increases transgene mRNA levels from rAAV and**
517 **lentiviral vectors.**

518 (A) rAAV2 tdTomato transgene mRNA levels in WT, MORC3 KO or SETDB1 KO A549 cells

519 normalized to 18S ribosomal RNA levels.

520 (B) Lentiviral GFP transgene mRNA levels in WT, MORC3 KO or SETDB1 KO A549 cells

521 normalized to 18S ribosomal RNA levels.

522 All data are shown as the mean ± s.e.m. from biological triplicates. P-values were determined

523 by an ordinary one-way ANOVA test and are defined as follows: ns: non-significant; *: <0.05; **:

524 <0.01; ***: <0.001; ****: <0.0001.

525

526 **Supplemental Table 1: MaGeCK analysis of A549 CRISPR KO and K562 CRISPRi screens for**

527 **increased AAV2 transgene expression.**

528

529 **Supplemental Table 2: Functional enrichment analysis for biological processes, molecular**

530 **function and cellular components of the STRING network containing the top 100 genes from**

531 **the A549 and K562 CRISPR screens.**

532

533 **Supplemental Table 3: DNA oligos used in this study.**

534

535

Figure 1

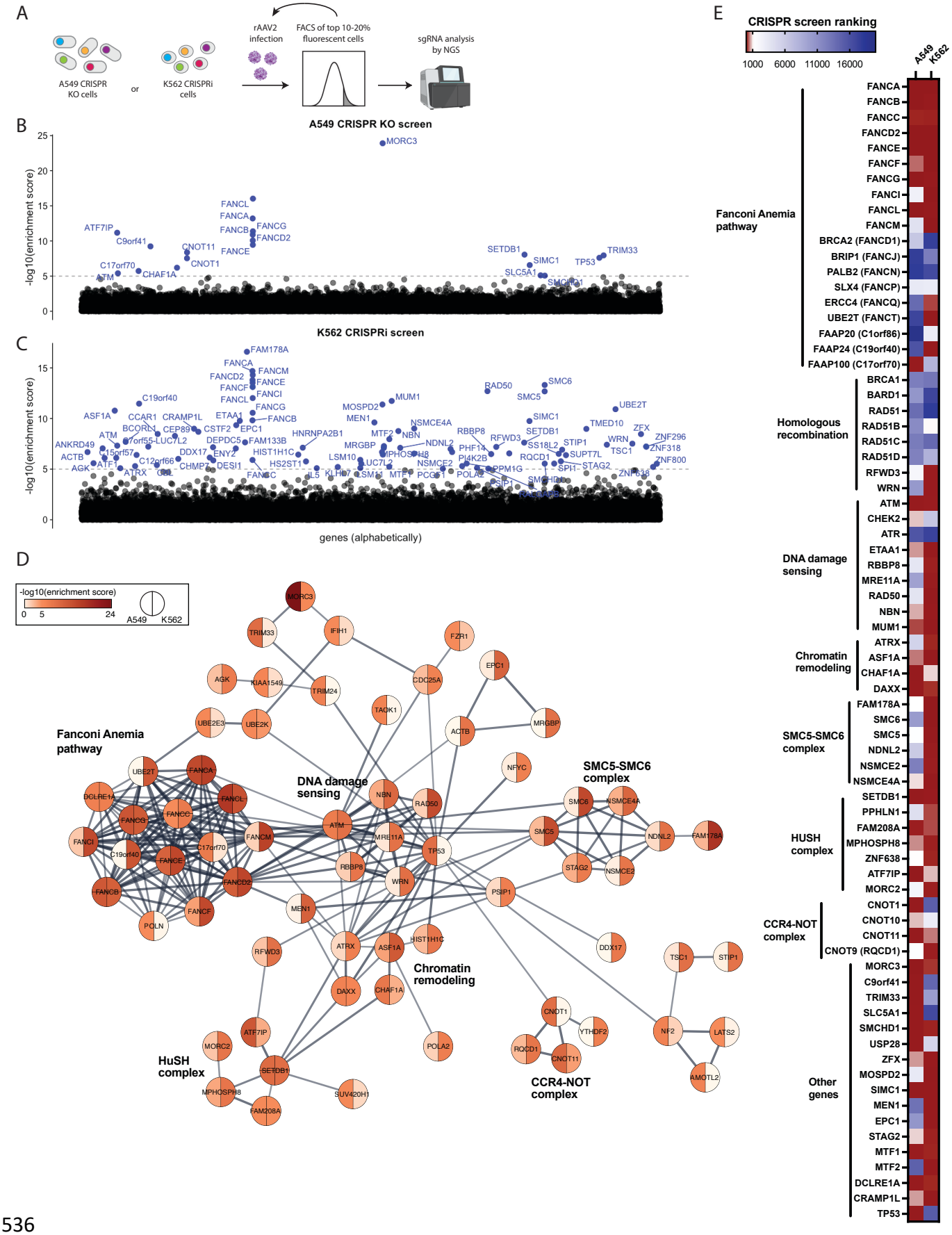
A
A549 CRISPR KO cells
or
K562 CRISPRi cells
rAAV2 infection
FACS of top 10-20% fluorescent cells
sgRNA analysis by NGS
B
A549 CRISPR KO screen
-log10(enrichment score)
C
K562 CRISPRi screen
genes (alphabetically)
D
-log10(enrichment score)
A549
K562
Fanconi Anemia pathway
DNA damage sensing
SMC5-SMC6 complex
Chromatin remodeling
HuSH complex
CCR4-NOT complex
E
CRISPR screen ranking
1000 6000 11000 16000
A549
K562
Fanconi Anemia pathway
Homologous recombination
DNA damage sensing
Chromatin remodeling
SMC5-SMC6 complex
HUSH complex
CCR4-NOT complex
Other genes

Figure 2

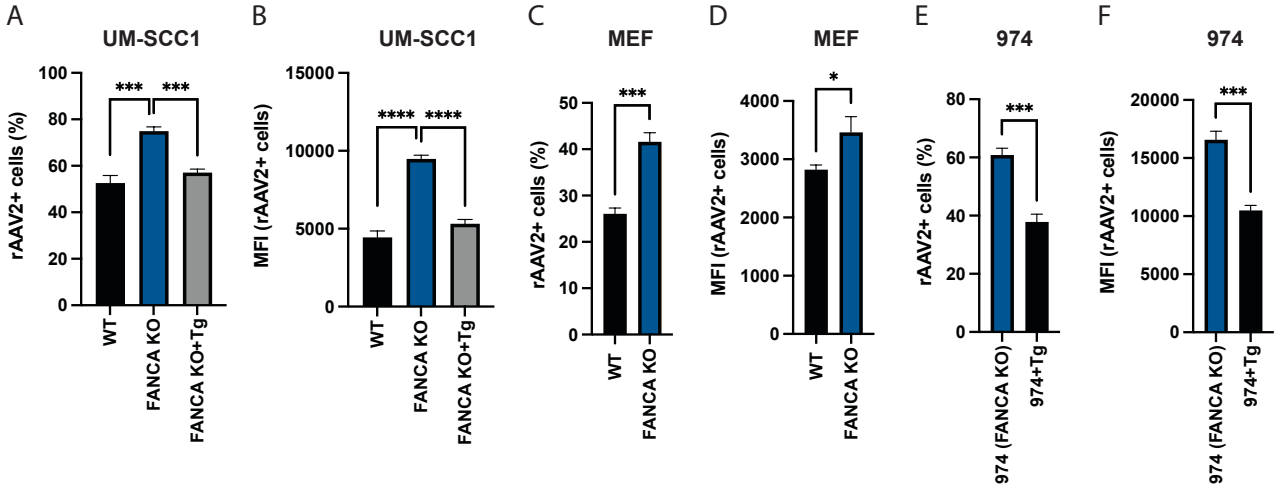
A
UM-SCC1
rAAV2+ cells (%)
100
80
60
40
20
0
***
***
WT
FANCA KO
FANCA KO+Tg
B
UM-SCC1
MFI (rAAV2+ cells)
15000
10000
5000
0
****
****
WT
FANCA KO
FANCA KO+Tg
C
MEF
rAAV2+ cells (%)
50
40
30
20
10
0
***
WT
FANCA KO
D
MEF
MFI (rAAV2+ cells)
4000
3000
2000
1000
0
*
WT
FANCA KO
E
974
rAAV2+ cells (%)
80
60
40
20
0
***
974 (FANCA KO)
974+Tg
F
974
MFI (rAAV2+ cells)
20000
15000
10000
5000
0
***
974 (FANCA KO)
974+Tg

537

Figure 3

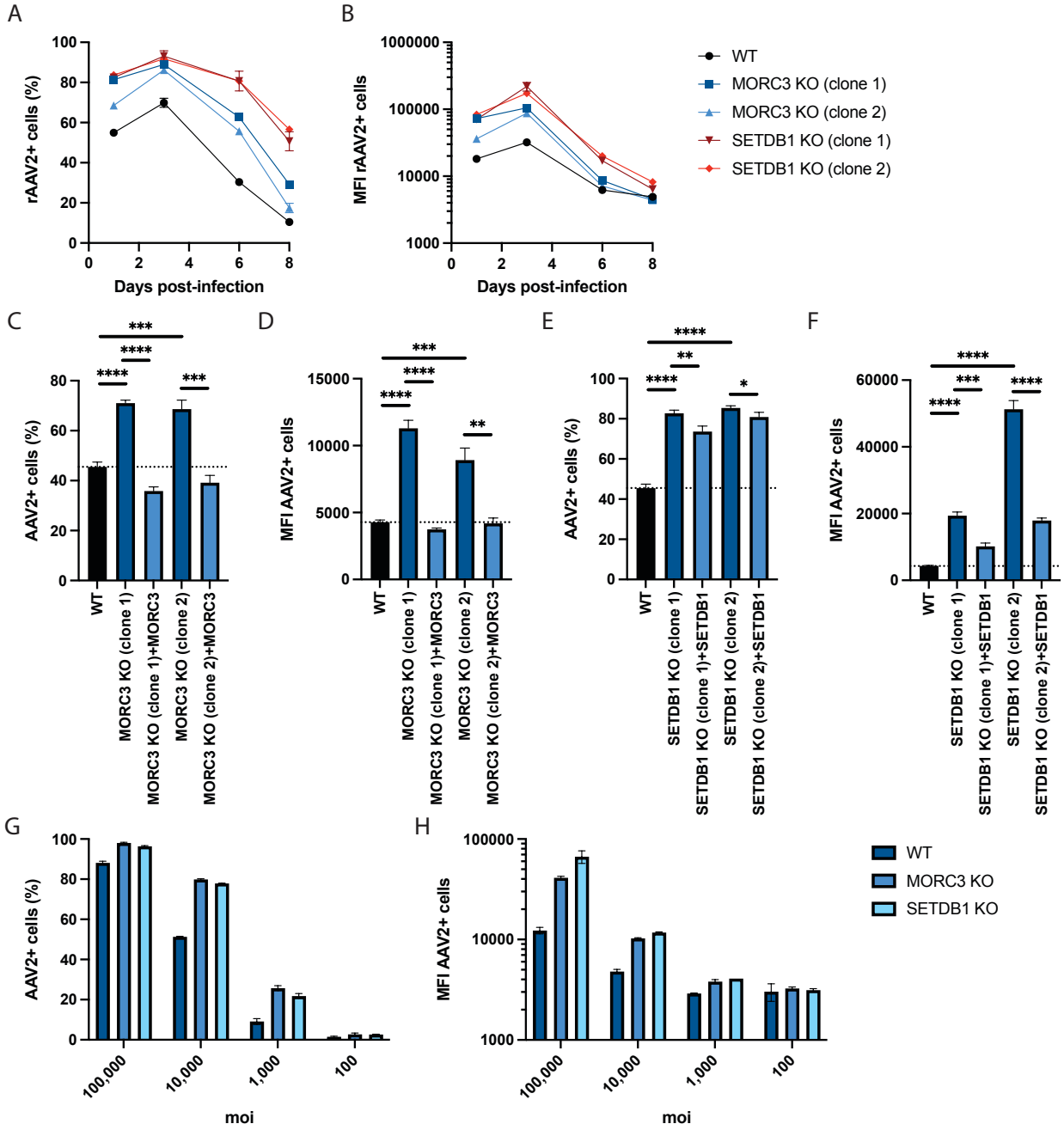
A
rAAV2+ cells (%)
Days post-infection
B
MFI rAAV2+ cells
Days post-infection
WT
MORC3 KO (clone 1)
MORC3 KO (clone 2)
SETDB1 KO (clone 1)
SETDB1 KO (clone 2)
C
AAV2+ cells (%)
WT
MORC3 KO (clone 1)
MORC3 KO (clone 1)+MORC3
MORC3 KO (clone 2)
MORC3 KO (clone 2)+MORC3
D
MFI AAV2+ cells
WT
MORC3 KO (clone 1)
MORC3 KO (clone 1)+MORC3
MORC3 KO (clone 2)
MORC3 KO (clone 2)+MORC3
E
AAV2+ cells (%)
WT
SETDB1 KO (clone 1)
SETDB1 KO (clone 1)+SETDB1
SETDB1 KO (clone 2)
SETDB1 KO (clone 2)+SETDB1
F
MFI AAV2+ cells
WT
SETDB1 KO (clone 1)
SETDB1 KO (clone 1)+SETDB1
SETDB1 KO (clone 2)
SETDB1 KO (clone 2)+SETDB1
G
AAV2+ cells (%)
100,000
10,000
1,000
100
moi
H
MFI AAV2+ cells
100,000
10,000
1,000
100
moi
WT
MORC3 KO
SETDB1 KO

538

Figure 4

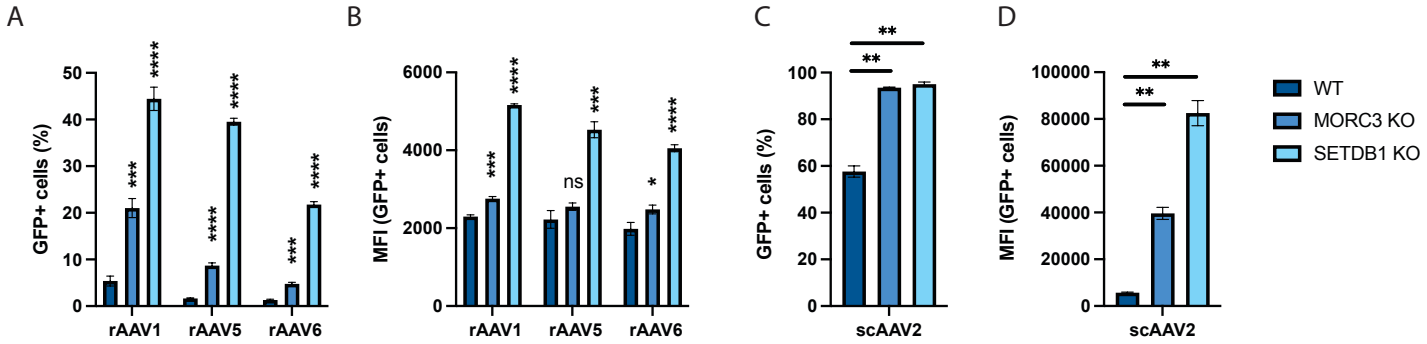
A
B
C
D
GFP+ cells (%)
MFI (GFP+ cells)
rAAV1
rAAV5
rAAV6
scAAV2
ns
WT
MORC3 KO
SETDB1 KO

539

Figure 5

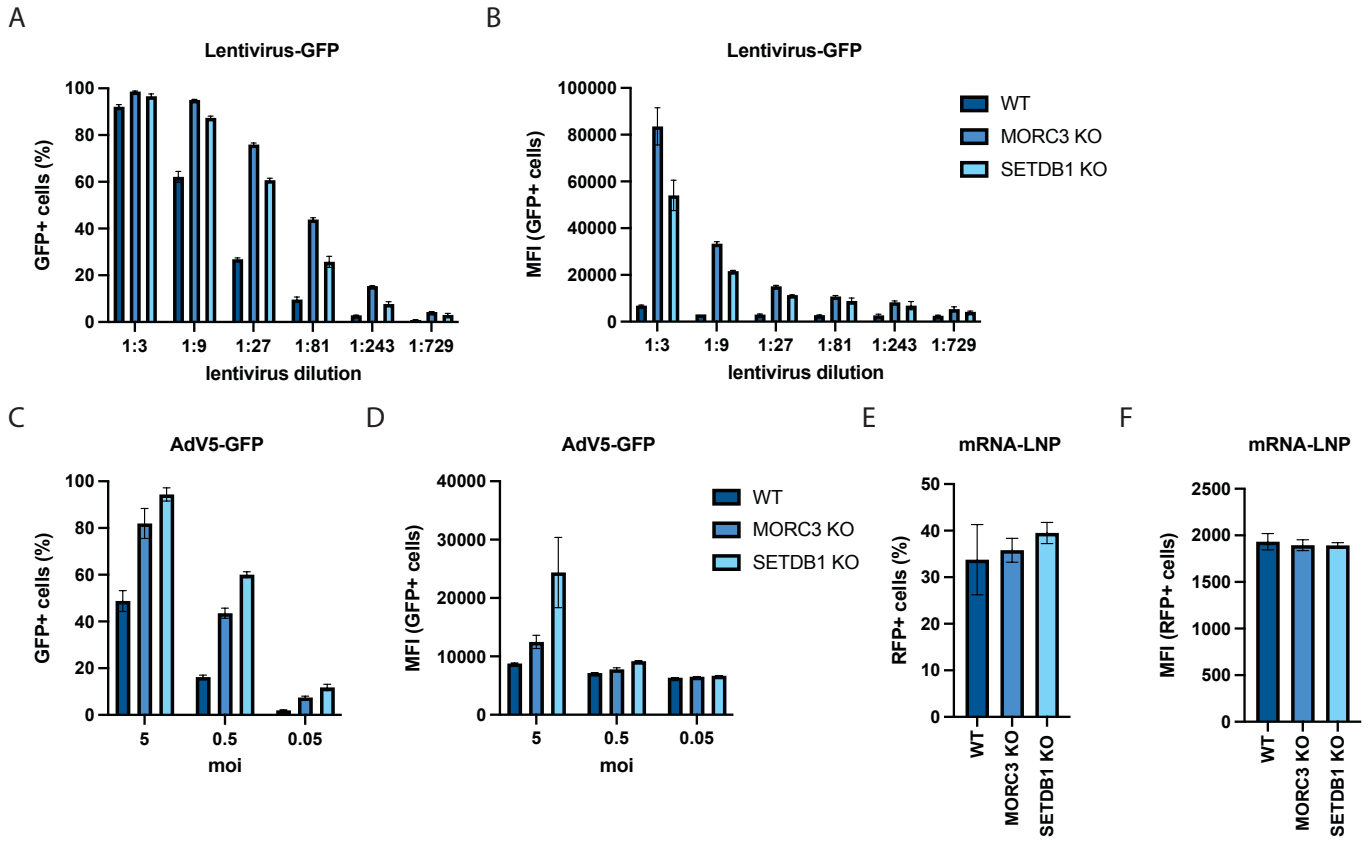
A
Lentivirus-GFP
GFP+ cells (%)
100
80
60
40
20
0
1:3
1:9
1:27
1:81
1:243
1:729
lentivirus dilution
B
Lentivirus-GFP
MFI (GFP+ cells)
100000
80000
60000
40000
20000
0
1:3
1:9
1:27
1:81
1:243
1:729
lentivirus dilution
WT
MORC3 KO
SETDB1 KO
C
AdV5-GFP
GFP+ cells (%)
100
80
60
40
20
0
5
0.5
0.05
moi
D
AdV5-GFP
MFI (GFP+ cells)
40000
30000
20000
10000
0
5
0.5
0.05
moi
WT
MORC3 KO
SETDB1 KO
E
mRNA-LNP
RFP+ cells (%)
50
40
30
20
10
0
WT
MORC3 KO
SETDB1 KO
F
mRNA-LNP
MFI (RFP+ cells)
2500
2000
1500
1000
500
0
WT
MORC3 KO
SETDB1 KO

540

Figure 6

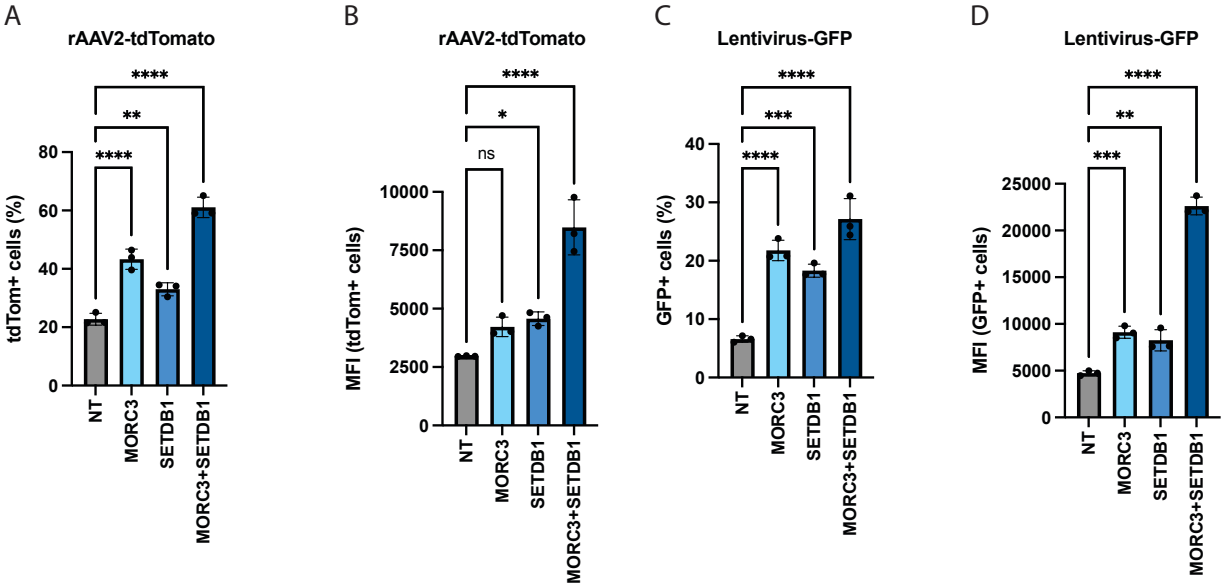
A
rAAV2-tdTomato
tdTom+ cells (%)
0
20
40
60
80
****
**
****
NT
MORC3
SETDB1
MORC3+SETDB1
B
rAAV2-tdTomato
MFI (tdTom+ cells)
0
2500
5000
7500
10000
****
*
ns
NT
MORC3
SETDB1
MORC3+SETDB1
C
Lentivirus-GFP
GFP+ cells (%)
0
10
20
30
40
****
***
****
NT
MORC3
SETDB1
MORC3+SETDB1
D
Lentivirus-GFP
MFI (GFP+ cells)
0
5000
10000
15000
20000
25000
****
**
***
NT
MORC3
SETDB1
MORC3+SETDB1

541

Figure S1

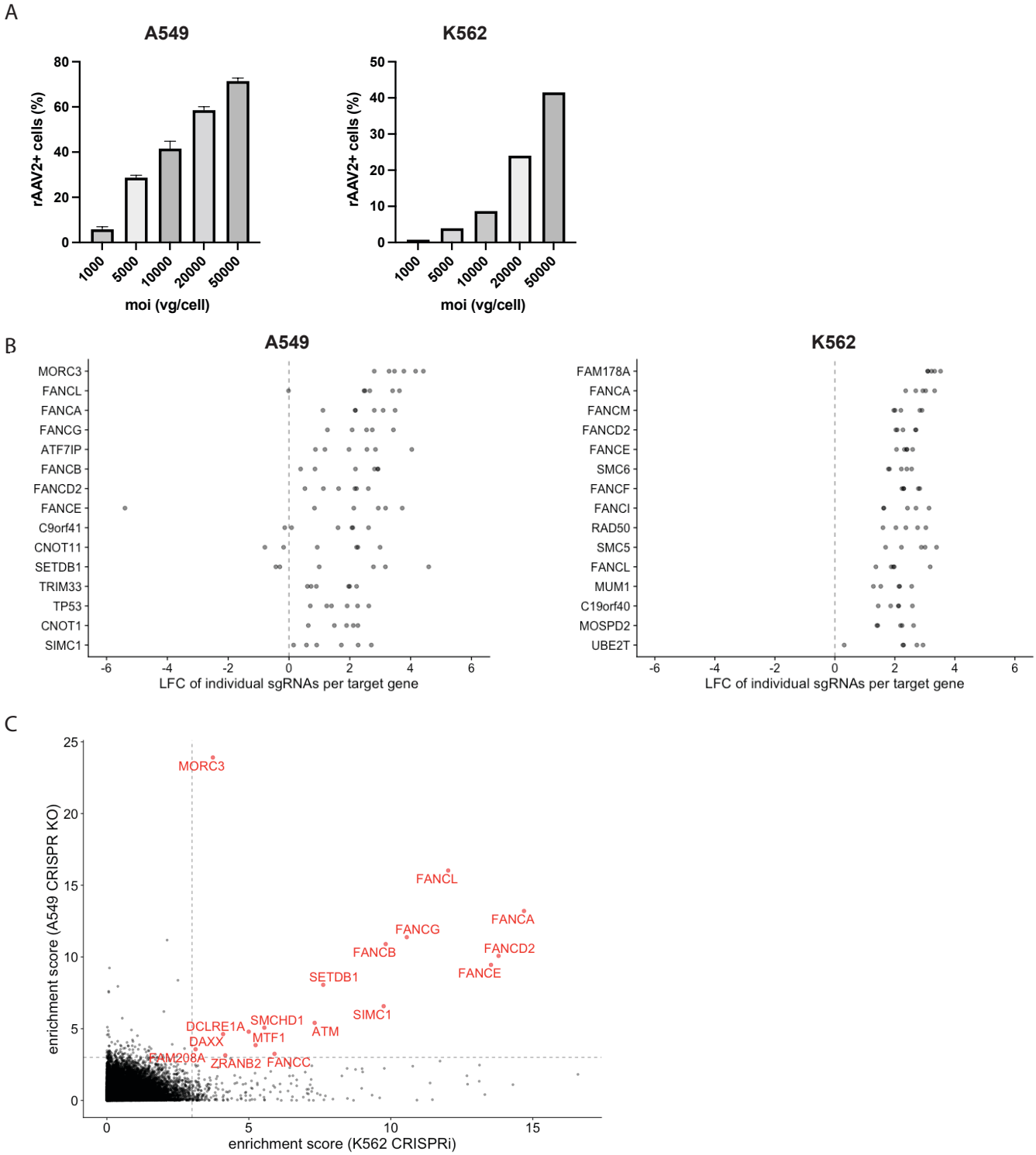

542

Figure S2

A

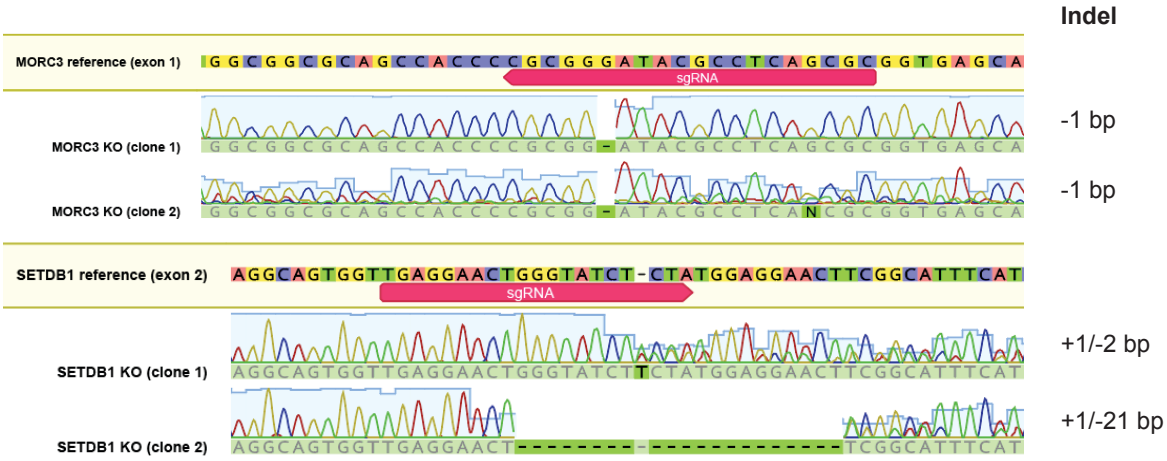

B

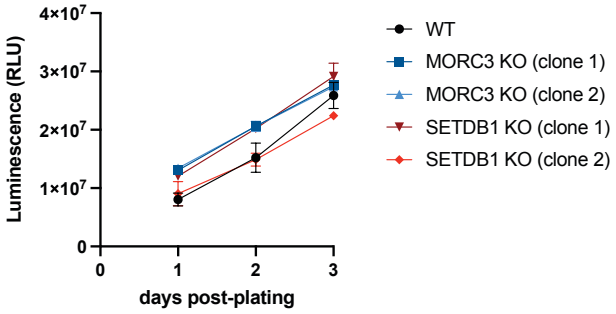

543

Figure S3

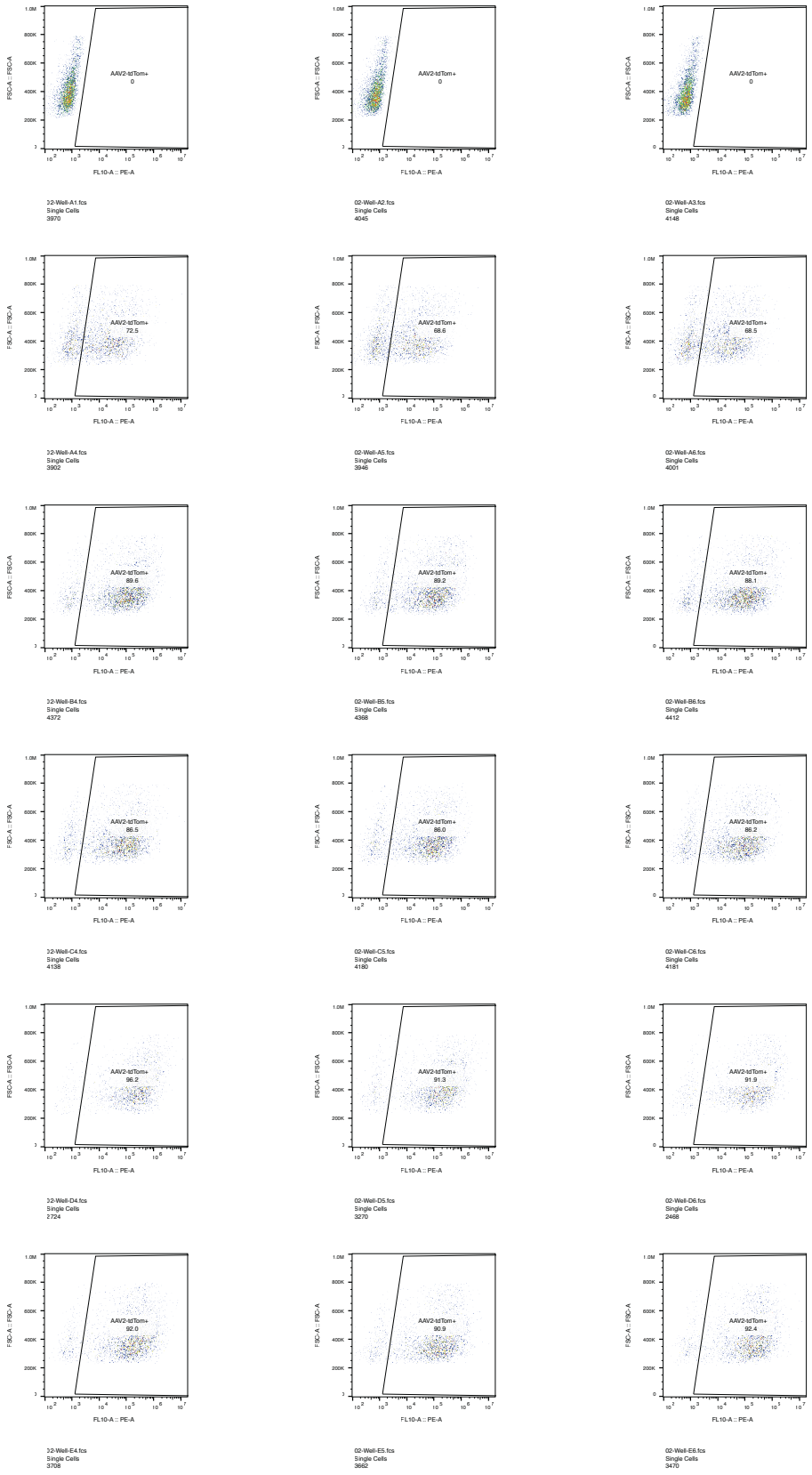

Uninfected

WT A549 + AAV2

MORC3 KO (clone 1) + AAV2

MORC3 KO (clone 2) + AAV2

SETDB1 KO (clone 1) + AAV2

SETDB1 KO (clone 2) + AAV2

544

Figure S4

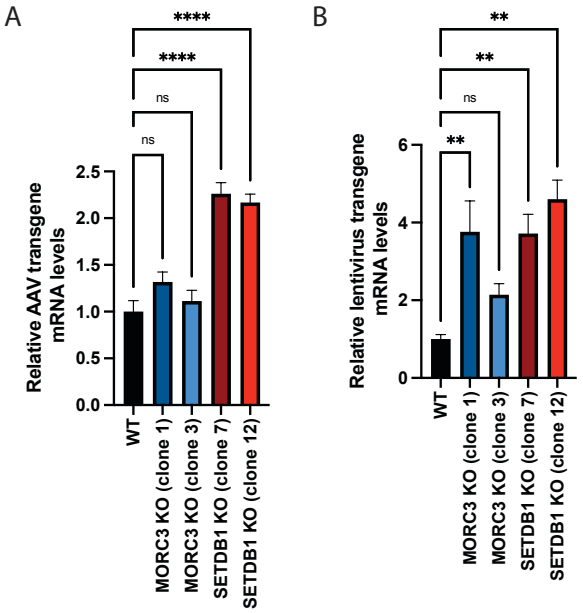

545

546

547 **REFERENCES**

548 1. Srivastava, A., Lusby, E.W., and Berns, K.I. (1983). Nucleotide sequence and organization of
549 the adeno-associated virus 2 genome. J Virol *45*, 555–564.

550 2. Samulski, R.J., and Muzyczka, N. (2014). AAV-Mediated Gene Therapy for Research and
551 Therapeutic Purposes. Annu Rev Virol *1*, 427–451.

552 3. McLaughlin, S.K., Collis, P., Hermonat, P.L., and Muzyczka, N. (1988). Adeno-associated virus
553 general transduction vectors: analysis of proviral structures. J Virol *62*, 1963–1973.

554 4. Wang, D., Tai, P.W.L., and Gao, G. (2019). Adeno-associated virus vector as a platform for
555 gene therapy delivery. Nat Rev Drug Discov *18*, 358–378.

556 5. Colella, P., Ronzitti, G., and Mingozzi, F. (2018). Emerging Issues in AAV-Mediated In Vivo
557 Gene Therapy. Molecular Therapy - Methods & Clinical Development *8*, 87–104.

558 6. Greig, J.A., Breton, C., Martins, K.M., Zhu, Y., He, Z., White, J., Bell, P., Wang, L., and Wilson,
559 J.M. (2022). Loss of transgene expression limits liver gene therapy in primates.
560 2022.03.24.485675.

561 7. Ceccaldi, R., Sarangi, P., and D'Andrea, A.D. (2016). The Fanconi anaemia pathway: new
562 players and new functions. Nat Rev Mol Cell Biol *17*, 337–349.

563 8. Maréchal, A., and Zou, L. (2013). DNA Damage Sensing by the ATM and ATR Kinases. Cold
564 Spring Harb Perspect Biol *5*, a012716.

565 9. Cai, M.-Y., Dunn, C.E., Chen, W., Kochupurakkal, B.S., Nguyen, H., Moreau, L.A., Shapiro, G.I.,
566 Parmar, K., Kozono, D., and D'Andrea, A.D. (2020). Cooperation of the ATM and Fanconi
567 Anemia/BRCA Pathways in Double-Strand Break End Resection. Cell Reports *30*, 2402-
568 2415.e5.

569 10. Aragón, L. (2018). The Smc5/6 Complex: New and Old Functions of the Enigmatic Long-
570 Distance Relative. Annu Rev Genet *52*, 89–107.

571 11. Tchasovnikarova, I.A., Timms, R.T., Matheson, N.J., Wals, K., Antrobus, R., Göttgens, B.,
572 Dougan, G., Dawson, M.A., and Lehner, P.J. (2015). Epigenetic silencing by the HUSH complex
573 mediates position-effect variegation in human cells. Science *348*, 1481–1485.

574 12. Liu, N., Lee, C.H., Swigut, T., Grow, E., Gu, B., Bassik, M.C., and Wysocka, J. (2018).
575 Selective silencing of euchromatic L1s revealed by genome-wide screens for L1 regulators.
576 Nature *553*, 228–232.

577 13. Tchasovnikarova, I.A., Timms, R.T., Douse, C.H., Roberts, R.C., Dougan, G., Kingston, R.E.,
578 Modis, Y., and Lehner, P.J. (2017). Hyperactivation of HUSH complex function by Charcot-
579 Marie-Tooth disease mutation in MORC2. Nat Genet *49*, 1035–1044.

580 14. Timms, R.T., Tchasovnikarova, I.A., Antrobus, R., Dougan, G., and Lehner, P.J. (2016).
581 ATF7IP-Mediated Stabilization of the Histone Methyltransferase SETDB1 Is Essential for
582 Heterochromatin Formation by the HUSH Complex. Cell Rep *17*, 653–659.

583 15. Zhu, Y., Wang, G.Z., Cingöz, O., and Goff, S.P. (2018). NP220 mediates silencing of
584 unintegrated retroviral DNA. Nature *564*, 278–282.

585 16. Moissiard, G., Cokus, S.J., Cary, J., Feng, S., Billi, A.C., Stroud, H., Husmann, D., Zhan, Y.,
586 Lajoie, B.R., McCord, R.P., et al. (2012). MORC family ATPases required for heterochromatin
587 condensation and gene silencing. Science *336*, 1448–1451.

588 17. Sloan, E., Orr, A., and Everett, R.D. (2016). MORC3, a Component of PML Nuclear Bodies,
589 Has a Role in Restricting Herpes Simplex Virus 1 and Human Cytomegalovirus. Journal of
590 Virology *90*, 8621–8633.

591 18. Groh, S., Milton, A.V., Marinelli, L.K., Sickinger, C.V., Russo, A., Bollig, H., de Almeida,
592 G.P., Schmidt, A., Forné, I., Imhof, A., et al. (2021). Morc3 silences endogenous retroviruses
593 by enabling Daxx-mediated histone H3.3 incorporation. Nat Commun *12*, 5996.

594 19. Webster, A.L.H., Sanders, M.A., Patel, K., Dietrich, R., Noonan, R.J., Lach, F.P., White,
595 R.R., Goldfarb, A., Hadi, K., Edwards, M.M., et al. (2021). Fanconi Anemia Pathway Deficiency
596 Drives Copy Number Variation in Squamous Cell Carcinomas. 2021.08.14.456365.

597 20. Bulcha, J.T., Wang, Y., Ma, H., Tai, P.W.L., and Gao, G. (2021). Viral vector platforms
598 within the gene therapy landscape. Sig Transduct Target Ther *6*, 1–24.

599 21. Collins, P.L., Kyle, K.E., Egawa, T., Shinkai, Y., and Oltz, E.M. (2015). The histone
600 methyltransferase SETDB1 represses endogenous and exogenous retroviruses in B
601 lymphocytes. Proceedings of the National Academy of Sciences *112*, 8367–8372.

602 22. Zhang, M.M., Bahal, R., Rasmussen, T.P., Manautou, J.E., and Zhong, X.-B. (2021). The
603 growth of siRNA-based therapeutics: Updated clinical studies. Biochem Pharmacol *189*,
604 114432.

605 23. de Alencastro, G., Puzzo, F., Pavel-Dinu, M., Zhang, F., Pillay, S., Majzoub, K., Tiffany, M.,
606 Jang, H., Sheikali, A., Cromer, M.K., et al. (2021). Improved Genome Editing through
607 Inhibition of FANCM and Members of the BTR Dissolvase Complex. Mol Ther *29*, 1016–1027.

608 24. Zentilin, L., Marcello, A., and Giacca, M. (2001). Involvement of cellular double-stranded
609 DNA break binding proteins in processing of the recombinant adeno-associated virus
610 genome. J Virol *75*, 12279–12287.

611 25. Schwartz, R.A., Palacios, J.A., Cassell, G.D., Adam, S., Giacca, M., and Weitzman, M.D.
612 (2007). The Mre11/Rad50/Nbs1 complex limits adeno-associated virus transduction and
613 replication. J Virol *81*, 12936–12945.

614 26. Lentz, T.B., and Samulski, R.J. (2015). Insight into the mechanism of inhibition of adeno-
615 associated virus by the Mre11/Rad50/Nbs1 complex. J Virol *89*, 181–194.

616 27. Robbez-Masson, L., Tie, C.H.C., Conde, L., Tunbak, H., Husovsky, C., Tchasovnikarova,
617 I.A., Timms, R.T., Herrero, J., Lehner, P.J., and Rowe, H.M. (2018). The HUSH complex
618 cooperates with TRIM28 to repress young retrotransposons and new genes. Genome Res *28*,
619 836–845.

620 28. Wang, G.Z., and Goff, S.P. (2016). Transcriptional Silencing of Moloney Murine Leukemia
621 Virus in Human Embryonic Carcinoma Cells. J Virol *91*, e02075-16.

622 29. Smith-Moore, S., Neil, S.J.D., Fraefel, C., Linden, R.M., Bollen, M., Rowe, H.M., and
623 Henckaerts, E. (2018). Adeno-associated virus Rep proteins antagonize phosphatase PP1 to
624 counteract KAP1 repression of the latent viral genome. Proceedings of the National Academy
625 of Sciences *115*, E3529–E3538.

626 30. Das, A., Vijayan, M., Walton, E.M., Stafford, V.G., Fiflis, D.N., and Asokan, A. (2021).
627 Epigenetic silencing of recombinant AAV genomes by NP220 and the HUSH complex. J Virol,
628 JVI0203921.

629 31. Li, D.-Q., Nair, S.S., and Kumar, R. (2013). The MORC family. Epigenetics *8*, 685–693.

630 32. Xue, Y., Gibbons, R., Yan, Z., Yang, D., McDowell, T.L., Sechi, S., Qin, J., Zhou, S., Higgs, D.,
631 and Wang, W. (2003). The ATRX syndrome protein forms a chromatin-remodeling complex
632 with Daxx and localizes in promyelocytic leukemia nuclear bodies. Proc Natl Acad Sci U S A
633 *100*, 10635–10640.

634 33. Hoelper, D., Huang, H., Jain, A.Y., Patel, D.J., and Lewis, P.W. (2017). Structural and
635 mechanistic insights into ATRX-dependent and -independent functions of the histone
636 chaperone DAXX. Nat Commun *8*, 1193.

637 34. Volk, A., and Crispino, J.D. (2015). The role of the chromatin assembly complex (CAF-1)
638 and its p60 subunit (CHAF1b) in homeostasis and disease. Biochim Biophys Acta *1849*, 979–
639 986.

640 35. Geis, F.K., Sabo, Y., Chen, X., Li, Y., Lu, C., and Goff, S.P. (2022). CHAF1A/B mediate
641 silencing of unintegrated HIV-1 DNAs early in infection. Proceedings of the National Academy
642 of Sciences *119*, e2116735119.

643 36. Uhlmann, F. (2016). SMC complexes: from DNA to chromosomes. Nat Rev Mol Cell Biol
644 *17*, 399–412.

645 37. Yiu, S.P.T., Guo, R., Zerbe, C., Weekes, M.P., and Gewurz, B.E. (2022). Epstein-Barr virus
646 BNRF1 destabilizes SMC5/6 cohesin complexes to evade its restriction of replication
647 compartments. Cell Reports *38*.

648 38. Bentley, P., Tan, M.J.A., McBride, A.A., White, E.A., and Howley, P.M. (2018). The
649 SMC5/6 Complex Interacts with the Papillomavirus E2 Protein and Influences Maintenance of
650 Viral Episomal DNA. J Virol *92*, e00356-18.

651 39. Decorsière, A., Mueller, H., van Breugel, P.C., Abdul, F., Gerossier, L., Beran, R.K.,
652 Livingston, C.M., Niu, C., Fletcher, S.P., Hantz, O., et al. (2016). Hepatitis B virus X protein
653 identifies the Smc5/6 complex as a host restriction factor. Nature *531*, 386–389.

654 40. Dupont, L., Bloor, S., Williamson, J.C., Cuesta, S.M., Shah, R., Teixeira-Silva, A., Naamati,
655 A., Greenwood, E.J.D., Sarafianos, S.G., Matheson, N.J., et al. (2021). The SMC5/6 complex
656 compacts and silences unintegrated HIV-1 DNA and is antagonized by Vpr. Cell Host Microbe
657 *29*, 792-805.e6.

658 41. Räschle, M., Smeenk, G., Hansen, R.K., Temu, T., Oka, Y., Hein, M.Y., Nagaraj, N., Long,
659 D.T., Walter, J.C., Hofmann, K., et al. (2015). DNA repair. Proteomics reveals dynamic
660 assembly of repair complexes during bypass of DNA cross-links. Science *348*, 1253671.

661 42. Oravcová, M., Nie, M., Zilio, N., Maeda, S., Jami-Alahmadi, Y., Lazzerini-Denchi, E.,
662 Wohlschlegel, J.A., Ulrich, H.D., Otomo, T., and Boddy, M.N. (2022). The Nse5/6-like SIMC1-
663 SLF2 Complex Localizes SMC5/6 to Viral Replication Centers. 2022.05.17.492321.

664 43. Hölscher, C., Sonntag, F., Henrich, K., Chen, Q., Beneke, J., Matula, P., Rohr, K., Kaderali,
665 L., Beil, N., Erfle, H., et al. (2015). The SUMOylation Pathway Restricts Gene Transduction by
666 Adeno-Associated Viruses. PLOS Pathogens *11*, e1005281.

667 44. Mano, M., Ippodrino, R., Zentilin, L., Zacchigna, S., and Giacca, M. (2015). Genome-wide
668 RNAi screening identifies host restriction factors critical for in vivo AAV transduction.
669 Proceedings of the National Academy of Sciences *112*, 11276–11281.

670 45. Chougui, G., Munir-Matloob, S., Matkovic, R., Martin, M.M., Morel, M., Lahouassa, H.,
671 Leduc, M., Ramirez, B.C., Etienne, L., and Margottin-Goguet, F. (2018). HIV-2/SIV viral protein
672 X counteracts HUSH repressor complex. Nat Microbiol *3*, 891–897.

673 46. Domenger, C., and Grimm, D. (2019). Next-generation AAV vectors—do not judge a virus
674 (only) by its cover. Human Molecular Genetics *28*, R3–R14.

675 47. Sanjana, N.E., Shalem, O., and Zhang, F. (2014). Improved vectors and genome-wide
676 libraries for CRISPR screening. Nat. Methods *11*, 783–784.

677 48. Horlbeck, M.A., Gilbert, L.A., Villalta, J.E., Adamson, B., Pak, R.A., Chen, Y., Fields, A.P.,
678 Park, C.Y., Corn, J.E., Kampmann, M., et al. (2016). Compact and highly active next-
679 generation libraries for CRISPR-mediated gene repression and activation. Elife *5*, e19760.

680 49. Li, W., Xu, H., Xiao, T., Cong, L., Love, M.I., Zhang, F., Irizarry, R.A., Liu, J.S., Brown, M.,
681 and Liu, X.S. (2014). MAGeCK enables robust identification of essential genes from genome-
682 scale CRISPR/Cas9 knockout screens. Genome Biol. *15*, 554.

683 50. Szklarczyk, D., Gable, A.L., Nastou, K.C., Lyon, D., Kirsch, R., Pyysalo, S., Doncheva, N.T.,
684 Legeay, M., Fang, T., Bork, P., et al. (2021). The STRING database in 2021: customizable
685 protein-protein networks, and functional characterization of user-uploaded
686 gene/measurement sets. Nucleic Acids Res *49*, D605–D612.

687 51. Shannon, P., Markiel, A., Ozier, O., Baliga, N.S., Wang, J.T., Ramage, D., Amin, N.,
688 Schwikowski, B., and Ideker, T. (2003). Cytoscape: a software environment for integrated
689 models of biomolecular interaction networks. Genome Res *13*, 2498–2504.

690